External kink dynamics in classical $l = 2$ stellarators

R Ramasamy[1], K Aleynikova[2], N Nikulsin[3], M Hoelzl[1], F. Hindenlang[1] and the JOREK team

[1] *Max-Planck Institut für Plasmaphysik, Boltzmannstraße 2, 85748 Garching bei München*

[2] *Max-Planck Institut für Plasmaphysik, Wendelsteinstrasse 1, 17491 Greifswald*

[3] *Dept. of Astrophysical Sciences, Princeton University*

The nonlinear MHD code, JOREK [1], has been extended to include a stellarator reduced MHD model [2]. In this work, the code is used to model the nonlinear dynamics of external kink instabilities in classical $l = 2$ stellarator geometries with twofold periodicity and circular toroidally averaged cross section. Building on the analysis in [3], the dependence of the saturated perturbation amplitude on the fraction of external rotational transform, ι_{ext}, is investigated.

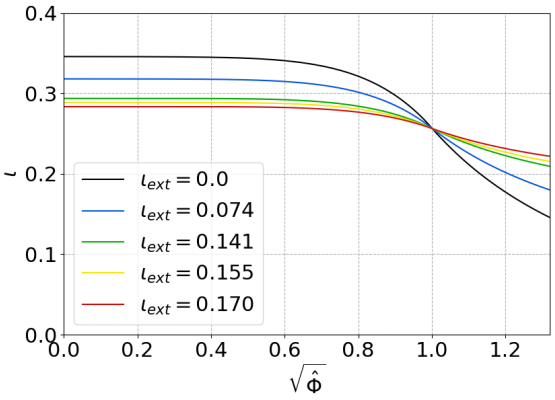

Figure 1: ι *profiles of* $l = 2$ *classical stellarators with varying* ι_{ext}*, keeping* ι_{edge} *constant.*

It is expected that as ι_{ext} is increased, the external kink will be stabilised. However, an open question is how the internal rational surfaces will respond to the flattening of the ι profile. For example, considering the ι profiles of the cases considered herein, shown in Figure 1, will the flattening of the ι profile around the $\iota = 2/7$ rational surface lead to exacerbated MHD activity, due to the triggering of secondary internal islands?

Extension of the JOREK code to study stellarators

For stellarators, the reduced MHD magnetic and velocity field ansatz are given by $\mathbf{B} = \nabla\chi + \nabla\psi \times \nabla\chi$ and $\mathbf{v} = \frac{\nabla\Phi\times\nabla\chi}{B_v^2}$, respectively, where $\nabla\chi$ represents the vacuum magnetic field generated by external currents. This ansatz neglects parallel flow, which is a second order quantity in the reduced ordering of high aspect ratio current driven external kink modes [5]. Defining $j = \Delta^*\psi$ as the plasma current along the direction of the vacuum magnetic field, and $\omega = \Delta^{\perp}\Phi$ as the plasma vorticity, the single temperature time evolution equations for the evolved variables for the poloidal flux, potential, density and temperature ($[\psi, \Phi, \rho, T]$) can be derived as

$$\frac{\partial \rho}{\partial t} = -B_v \left[\frac{\rho}{B_v^2}, \Phi\right] + \nabla \cdot \left(D_\perp \nabla_\perp \rho + D_\parallel \nabla_\parallel \rho\right) + S_\rho \tag{1}$$

$$\nabla\cdot\left(\frac{\rho}{B_v^2}\nabla^\perp\frac{\partial\Phi}{\partial t}\right)=\frac{B_v}{2}\left[\frac{\rho}{B_v^2},\frac{(\Phi,\Phi)}{B_v^2}\right]+B_v\left[\frac{\rho\omega}{B_v^4},\Phi\right]-\nabla\cdot\left(\frac{P}{B_v^2}\nabla^\perp\Phi\right)+\nabla\cdot(j\mathbf{B})+B_v\left[\frac{1}{B_v^2},p\right]+\nabla\cdot\left(\mu_\perp\nabla^\perp\omega\right)-\Delta^\perp\left(\mu_{num}\Delta^\perp\omega\right) \tag{2}$$

$$\rho\frac{\partial T}{\partial t}=-\frac{1}{B_v}[\rho T,\Phi]-\gamma\rho T B_v\left[\frac{1}{B_v^2},\Phi\right]+\nabla\cdot\left[\kappa_\perp\nabla_\perp T+\kappa_\parallel\nabla_\parallel T+\frac{pD_\perp}{\rho}\nabla_\perp\rho+\frac{pD_\parallel}{\rho}\nabla_\parallel\rho\right]+\left(S_e+\eta_{Ohm}B_v^2j^2\right)-T\frac{\partial\rho}{\partial t} \tag{3}$$

$$\frac{\partial\psi}{\partial t}=\frac{\partial^\parallel\Phi-[\psi,\Phi]}{B_v}-\eta\left(j-j_{source}\right)+\nabla\cdot\left(\eta_{num}\nabla^\perp j\right). \tag{4}$$

JOREK simulation set up and parameters

To model external kinks in JOREK, free boundary VMEC equilibria are extended into the vacuum region. Figure 2 shows how the computational boundary (grey) is shifted, such that it is sufficiently far from the plasma boundary (black) to observe the mode. The original plasma boundary (red dashed) from the computation without the extension of the domain is also shown to demonstrate that internal flux surfaces are not affected.

The viscoresistive and diffusive parameters used in simulations are shown in Table 1. A Spitzer-like resistivity is used to include a highly resistive vacuum region. The viscosity parameters are kept constant across the simulation domain to avoid damping the growth rate of the kink mode.

Table 1: *JOREK numerical and viscoresistive simulation parameters. Diffusive parameters are taken from the plasma core. Unless stated, values are in normalised JOREK units.*

Parameter	Value	Profile
$\kappa_\parallel$	1.0	Constant
$\kappa_\perp$	10^{-6}	Sigmoid
$D_\parallel$	0.01	Constant
$D_\perp$	10^{-6}	Sigmoid
$\eta\ [\Omega\cdot m]$	1.9382×10^{-7}	Spitzer
$\eta_{\text{num}}\ [\Omega\cdot m^3]$	1.9382×10^{-14}	Constant
$\mu\ [kg\cdot m^{-1}\cdot s^{-1}]$	5.1594×10^{-8}	Constant
$\mu_{\text{num}}\ [kgm\cdot s^{-1}]$	5.1594×10^{-15}	Constant
n_{rad}	64	—
n_{pol}	64	—
n_{tor}	12	—

In stellarator simulations, 64 poloidal and radial finite elements are used to represent a flux surface aligned grid, using 12 toroidal harmonics to represent both the full torus, non-axisymmetric grid and field variables. A subset of the simulations have been carried out at higher resolution with no significant difference in the observed nonlinear dynamics.

A constant parallel heat transport coefficient is also used to ease the toroidal resolution requirements - in stellarator simulations, it is observed that a large number of toroidal modes are necessary to accurately capture thermal transport. A parallel particle diffusivity is also applied to replace the parallel particle transport from advection, which has been neglected. Perpendicular particle and thermal diffusion coefficients are used in a similar way to [3], such that the vacuum region remains at low temperature and density. It should be noted that heat and particle sources were modified from case to case to ensure that similar stationary temperature and density profiles were obtained for all modeled case. After achieving these approximately stationary profiles, the instability is modeled by switching from a single period to a full torus simulation.

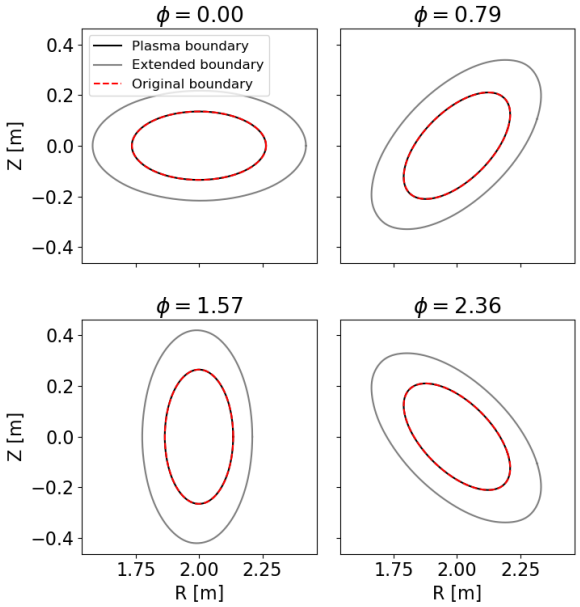

Figure 2: *Extended simulation domain imported to JOREK from VMEC.*

Influence of ι_{ext} on the nonlinear dynamics

To ensure the simulation set up is physically meaningful, the influence of ι_{ext} on the observed linear growth rate in JOREK (black) is shown in Figure 3. Comparing with results from free boundary CASTOR3D computations, it can be see that the predicted linear instability threshold from CASTOR3D (grey dashed) is approximately preserved in JOREK. The expected trend observed in previous work [3], that the linear growth rate decreases with increasing ι_{ext}, is also observed.

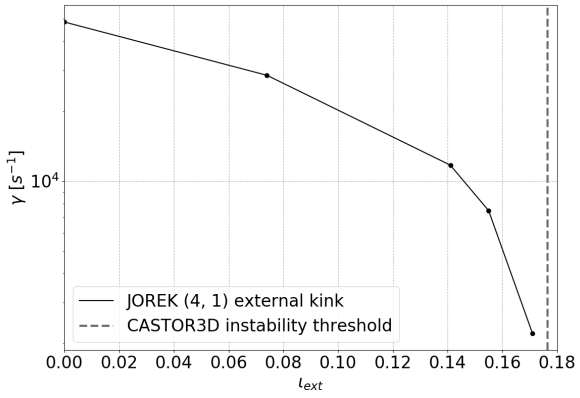

Figure 3: *Linear growth rates of the external kink mode as a function of* ι_{ext}.

Simulations are therefore continued into the nonlinear phase. A comparison of the loss in confinement between simulated cases is shown using Poincaré plots in Figure 4. In the limit of a tokamak, with no externally generated magnetic cage, significant confinement is lost within the plasma volume. Particularly, a (3, 1) magnetic island structure is observed, indicating that

secondary MHD activity has been triggered by the external kink. With increasing external rotational transform, as the current drive for the instability is reduced, the ergodisation induced by the saturated kink mode is mitigated. In such a way, field lines remain well confined for sufficiently high ι_{ext}. At approximately $\iota_{\text{ext}} = 0.170$, the external island structures no longer penetrate into the plasma volume, and although the internal surfaces are deformed appreciably, no secondary MHD modes are triggered.

Conclusion

The JOREK code has been used to show that the nonlinear dynamics of a (4, 1) external kink mode is stabilised by the influence of external helical currents in a classical $l = 2$ stellarator with circular toroidally averaged cross section. For the particular case simulated, the flattening of the q profile around low order rational surfaces does not exacerbate nonlinearly triggered modes. In fact, the removal of the $q = 3$ surface suppresses the (3, 1) mode activity observed in the tokamak case. This is not a general result, and ongoing work intends to understand when secondary mode activity can threaten the nonlinear MHD stability of stellarators.

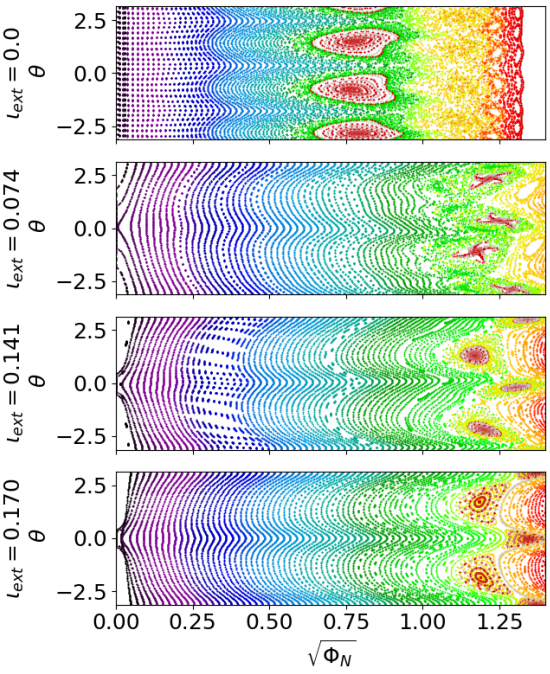

Figure 4: *Poincaré plots generated at the end of the simulation time for cases with different* ι_{ext}.

References

[1] M. Hoelzl, et al. Nuclear Fusion **61** 065001 (2021)
[2] N. Nikulsin, R. Ramasamy, M. Hoelzl et al. Physics of Plasmas **29** 063901 (2022).
[3] R. Ramasamy, et al. Physics of Plasmas **30**, 062506 (2023)
[4] E. Strumberger and S. Günter Nuclear Fusion **57** 016032 (2017)
[5] B. Kadomtsev, and O. Pogutse, Sov. Phys. JETP 5 575ž013590 (1973)

Acknowledgements

This work has been carried out within the framework of the EUROfusion Consortium, funded by the European Union via the Euratom Research and Training Programme (Grant Agreement No 101052200 — EUROfusion). Views and opinions expressed are however those of the authors only and do not necessarily reflect those of the European Union or the European Commission. Neither the European Union nor the European Commission can be held responsible for them.